



## Original article

## Establishing a mouse model of choroidal neovascularization to study the therapeutic effect of levatinib and its mechanism

Xiaonan Xin, Yueyu Zhu, Ruijie Xi, Yuhua Hao\*

Department of Ophthalmology, Second Hospital of Hebei Medical University, Shijiazhuang 050000, China



## ARTICLE INFO

## Article history:

Received 24 March 2020

Revised 13 June 2020

Accepted 22 June 2020

Available online 27 June 2020

## Keywords:

CNV

Levatinib

Retina

VEGF

Fluorescence leakage

## ABSTRACT

**Objective:** To study the therapeutic effect and mechanism of levatinib on choroidal neovascularization (CNV) in mice.

**Methods:** 45 healthy C57BL/6 mice were selected and randomly divided into three groups: control group (group A), model group (group B) and levatinib group (group C). The model of CNV in mice was established. The fluorescence leakage of choroidal lesions in mice was observed by fundus fluorescein angiography. The morphological changes of retinal vessels in mice were observed by retinal slice preparation, the pathological changes of eyeball tissues in mice were observed by hematoxylin-eosin (HE) staining, the expression of vascular endothelial growth factor (VEGF) in mice retina was detected by real-time quantitative fluorescence PCR, and the protein expression of VEGF in mice retina was detected by Western blotting.

**Result:** On the 7th, 14th and 21st day after modeling, compared with group B, the fluorescence leakage area of group C mice was significantly reduced, and the difference was statistically significant ( $P < 0.05$ ). The morphology of retinal vessels in group A was normal. In group B, the retinal vessels showed large areas of ischemia without perfusion and abundant neovascularization clusters and capillaries. Compared with group B, the morphology of retinal vessels in group C was significantly improved. Group A mice had normal eyeball structure, group B mice had visible spindle-like damage to the inner and outer retina, while group C mice had significantly less spindle-like damage than group B. Compared with group A, group B mice had significantly higher expression of retinal VEGF and the difference was statistically significant ( $P < 0.05$ ), but compared with group B mice, the expression of VEGF in the retina of mice in group C was significantly decreased, and the difference was statistically significant ( $P < 0.05$ ). Compared with group A, the expression of VEGF in retina of group B mice was significantly increased, and the difference was statistically significant ( $P < 0.05$ ). Compared with group B, the expression of VEGF in retina of group C mice was significantly decreased, and the difference was statistically significant ( $P < 0.05$ ).

**Conclusion:** Levatinib has obvious therapeutic effect on CNV, which may be achieved by inhibiting the high expression of VEGF in CNV.

© 2020 The Authors. Published by Elsevier B.V. on behalf of King Saud University. This is an open access article under the CC BY-NC-ND license (<http://creativecommons.org/licenses/by-nc-nd/4.0/>).

## 1. Introduction

Choroidal neovascularization (CNV) is formed by the proliferating vessels of choroidal capillaries extending to the cleft of the vitreous membrane. It can occur between the nerve retina and the

retinal pigment epithelium, between the vitreous membrane and the retinal pigment epithelium, and between the retinal pigment epithelium and the choroid (Philip et al., 2019; Zhao et al., 2019). Many diseases affecting retinal pigmented epithelium-vitreous membrane-choroidal capillary can lead to the formation of CNV. These diseases include age-related macular degeneration, hereditary macular degeneration, pseudo-ocular histoplasmosis syndrome, choroidal pigmented nevus and choroidal rupture (Saurabh et al., 2018; Lima et al., 2019; Rust et al., 2019). In the early stage of CNV, there are usually no conscious symptoms (Aggarwal et al., 2019). With the development of the disease, it can cause visual impairment, visual distortion or central dark spot (Kumar et al., 2018). In general fundus examination, the manifestation is subretinal hemorrhage and lipid-like exudation. Cystic

\* Corresponding author at: Department of Ophthalmology, Second Hospital of Hebei Medical University, 215 West Heping Road, Shijiazhuang, 050000, China.

E-mail address: [haoyuhua@126.com](mailto:haoyuhua@126.com) (Y. Hao).

Peer review under responsibility of King Saud University.



Production and hosting by Elsevier

macular edema can be seen in patients with a long course of disease (Hachana et al., 2020). CNV is usually seen in the macula, so the disease is also one of the main causes of blindness, causing serious damage to central vision (Haas et al., 2020). The disease often occurs in the eyes of adults, especially those aged over 60 years old, and should be detected and treated in time (Choudhary et al., 2018). At present, the main treatment for preventing the progression of CNV and reducing the pathological process of incomplete vascular leakage is intravitreal injection of anti-VEGF drugs (Murakawa et al., 2019). However, multiple intravitreal injections of such anti-VEGF drugs are likely to cause side effects such as increased intraocular pressure, retinal detachment, eye infections, and poor patient compliance (Park et al., 2019). Therefore, at present, one of the new research directions for the treatment of this kind of fundus diseases is to develop new drugs with potential therapeutic value. The main research directions of retinal diseases and CNV are non-invasive drug delivery and the development of new dosage forms and new drugs that can quickly pass through the blood-retinal barrier (Wang et al., 2019). Small molecular compounds with anti-vascular effects have potential development value for fundus medicine because of their rich targets and small molecular weight. Although commonly used anti-tumor drugs such as sunitinib and sorafenib have excellent anti-vascular effects, it is difficult to develop for the treatment of fundus neovascular diseases. The reasons include the blood-retinal barrier effect and the toxic side effects (Schwarzer et al., 2020). Therefore, for the treatment of CNV, the screening of a safe and effective small molecule compound is the focus of research.

Tyrosine kinase inhibitors (TKI) are a class of compounds that can inhibit the activity of tyrosine kinase. They can be used as competitive inhibitors of adenosine triphosphate (ATP) binding to tyrosine kinase or as analogues of tyrosine to block the activity of tyrosine kinase and inhibit cell proliferation (Kiel et al., 2020; Simhaee et al., 2020; Xiao et al., 2020). Levatinib is a multi-target tyrosine kinase receptor inhibitor (Mandal and Lotery, 2019). At present, levatinib has been approved by the Food and Drug Administration for the treatment of differentiated thyroid cancer and renal epithelial cell carcinoma. Also, it has achieved ideal clinical results (Gualino et al., 2019). It can inhibit other angiogenesis-related tyrosine kinases involved in tumor proliferation and selectively inhibit the activity of vascular endothelial growth factor (VEGF) receptor kinase (Savastano et al., 2019; Breazzano et al., 2020). Studies have shown that levatinib is effective in the treatment of anti-angiogenesis. It can inhibit angiogenesis by inhibiting the activation of VEGF2R, suggesting that levatinib may also be effective in the treatment of fundus angiogenesis-related diseases (Farinha et al., 2020; Moulton et al., 2020).

In summary, there are many studies on the application of levatinib in anti-angiogenesis, but there are few studies on CNV. In order to further understand the therapeutic effect of levatinib, 45 healthy and clean C57BL/6 mice were selected as the research objects to explore the therapeutic effect of levatinib on CNV in mice and its mechanism, which provides reference for clinical treatment of CNV.

## 2. Materials and methods

### 2.1. Research objects

45 healthy and clean C57BL/6 mice (XXX Animal Center), 8 weeks old and weighed about 20 g. All animals were fed in cages with rodents of national standard, with 4 animals per cage. They were free to drink water and eat. There was no significant difference in body weight between groups. Natural light and free diet were given. The temperature of the room was controlled at 20 ~ 26°C, and the humidity was controlled at 40 ~ 50%. The adaptive breeding was carried out

for 2 weeks. The operation of animal experiments conforms to the International Regulations on the Protection and Management of Animals and is approved by the ethical committee.

### 2.2. Establishment of a mouse model of CNV

Grouping: 45 C57BL/6 mice were randomly divided into three groups (15 mice in each group): control group (group A), model group (group B) and levatinib group (group C).

Modeling: 8-week-old mature C57BL/6 mice were small and easy to control. The eyeballs were similar to humans, and the choroid was pigmented. Therefore, they were commonly used model animals for ocular fundus neovascular disease. High-energy laser was used to photocoagulate the retina, destroying bruch's membrane. Then, secondary damage repair reaction and inflammation occurred. Choroidal epithelial cells, pericytes, fibroblasts, and inflammatory cells entered the subretinal space to form CNV. The specific modeling steps are as follows: Group B and group C mice were injected with chloral hydrate solution (10%, Shanghai Jingke Chemistry Technology Co., Ltd., China) at a dose of 3 mL/kg intraperitoneally. The mice were dilated three times with tropicamide (Beijing Shuanghe Modern Medical Technology Co., Ltd., China). The parameters of laser instrument (Tianjin Meida Medical Science and Technology Co., Ltd., China) are as follows: laser wavelength is 532 nm, power is 150mW, spot diameter is 100 μm, and exposure time is 0.1 s. Fix the mice in front of the slit lamp, and fully open the upper and lower eyelids. Laser was used to coagulate the mice from 3, 6, 9 and 12 o'clock directions at the 1PD distance from the optic disc. Both eyes of mice were modeled. When bubbles were formed, the glass membrane was broken down and the modelling was successful. Erythromycin eye ointment (Beijing Shuangji Pharmaceutical Co., Ltd., China) was applied to the eyes of mice. Group A mice were fed normally without any treatment.

Drug administration: Levatinib (Nanjing Xize Pharmaceutical Technology Co., Ltd., China) was prepared with 5% methylcellulose – 0.5 Tween 80. Group C mice were fed with levatinib at a dose of 100 μL per day, group B mice were fed with 5% methylcellulose-0.5 Tween 80 at the same dose per day, and group A mice were fed normally without any treatment.

Treatment of mice: Each group of mice was randomly divided into five subgroups (3 mice in each subgroup). They were used for fundus fluorescence angiography, retinal paving, hematoxylin-eosin (HE) staining, real-time quantitative fluorescent PCR, and protein immunoblotting, respectively. In real-time quantitative fluorescent PCR and Western blotting, the mice were killed firstly. After removing cornea, lens, vitreous, sclera and choroid, the retina was free and stored in –80 °C for reserve.

### 2.3. Observation of fluorescence leakage in choroidal lesions of mice by fundus fluorescein angiography

Fundus fluorescein angiography: On the 7th, 14th and 21st day after modeling, 10% chloral hydrate solution was intraperitoneally injected at a dose of 3 mL/kg. After anesthesia in mice, sodium fluorescein (4%, Shanghai Shifeng Biotechnology Co., Ltd., China) was intraperitoneally injected at a dose of 5 mL/kg.

Observation measures: Fluorescence leakage and laser damage in choroidal lesions of mice were observed by fundus fluorescence contrast apparatus (Heidelberg, Germany), and the area of fluorescence leakage was evaluated.

### 2.4. Morphological changes of retinal vessels in mice observed by retinal paving

Retinal paving: After anesthesia, the thoracic cavity of mice was opened, the heart was exposed, and a small amount of dextran

isothiocyanate fluorescein (Shanghai Yuanye Biotechnology Co., Ltd., China) was pushed into the left ventricle of mice for perfusion. Remove the mouse's eyeballs and place them in polyformaldehyde (4%, Shanghai Bairui Biotechnology Co., Ltd., China) and put it in dark conditions for 3 h. The retina was separated under the ophthalmic microscope (Leica, Germany) and paved.

Observation: The morphological changes of retinal vessels in mice were observed under fluorescence microscopy (Leica, Germany) and preserved by photography.

#### 2.5. Observation of pathological changes in eyeball tissue of mice by HE staining

Section production: After the mice were killed, their eyeballs were removed and completely covered with OCT embedding agent (Beijing Xinhua Green Source Technology Co., Ltd.) and frozen for 30 min. Eye tissue was sectioned continuously at a thickness of 5  $\mu$ m and fixed with acetone 30 min later. After 5 min, wash 3 times with phosphate buffer solution for 5 min each time.

Dyeing: 10 min later, dye with HE (Shanghai Baoman Biotechnology Co., Ltd., China) for 1 min and rinse with running water for 1 min. Add 1% ethanol hydrochloride to differentiate for 5 s and rinse with running water for 6 min. Eosin solution (Beijing Dingguo Changsheng Biotechnology Co., Ltd., China) was added to dye for 1 min, flushed for 1 min, and excess moisture was absorbed from filter paper. After gradient alcohol dehydration, xylene decolorization and transparency, take neutral gum (Shanghai Yantuo Biotechnology Co., Ltd., China) to seal it.

Observation: Morphological changes of Achilles tendon tissue were observed under light microscopy (Leica, Germany) and preserved by photography.

#### 2.6. RNA Extraction of total RNA from mouse retina by Trizol method

Take 50 mg retina, add 1 mL Trizol (Jiaozuolu Feifang Biotechnology Co., Ltd., China), and make ultrasound homogenate. Add 200  $\mu$ L of trichloromethane (Pharmaceutical Group Chemical Reagents Co., Ltd., China), cover the pipe cap and shake it vigorously to make it mix evenly. High-speed centrifuge (Allegra X-22, Beckman Kurt Co., Ltd., USA) was used to centrifuge (12,000 rpm, 4 °C) for 5 min. Absorb the upper solution and transfer it to the new EP tube, and add isopropanol (Tianjin Guangcheng Chemical Reagent Co., Ltd., China) in a ratio of 1:1. Waiting for 5 min at room temperature, centrifuge (12,000 rpm, 4 °C) for 2 min. Discard the supernatant and add 50  $\mu$ L DEPC water to dissolve it.

#### 2.7. Detection of the expression of VEGF in mouse retina by real-time PCR

Reverse transcription reaction: Total RNA template extracted by 1  $\mu$ g Trizol method was used as template, and 1  $\mu$ L random primers were added. The reaction lasted 15 min at 65 °C. The total volume was supplemented to 20  $\mu$ L by adding 4  $\mu$ L 5\*Buffer, 3  $\mu$ L dNTP, 1  $\mu$ L RNA enzyme inhibitor, 1  $\mu$ L reverse transcriptase and RNase Free dH<sub>2</sub>O. The reaction lasted 10 min at 25 °C, and 60 min and 15 min at 42 °C and 75 °C, respectively.

PCR reaction: The primer sequence of VEGF was designed, and the PCR reaction solution was added. Pre-denaturation was performed for 10 min at 94 °C, and Tag enzyme was activated. The reaction lasted 15 s under 94 °C and 60 s under 60 °C, and 45 cycles were repeated.

Computing method: The relative value of gene expression was calculated by 2<sup>- $\Delta\Delta$ CT</sup> method (with  $\beta$ -actin as internal reference).  $\Delta$ Ct = target gene Ct value - control gene Ct value,  $\Delta\Delta$ Ct = test sample  $\Delta$ Ct - control sample  $\Delta$ Ct. 2<sup>- $\Delta\Delta$ CT</sup> = the relative expression multiple  $\Delta$  of the tested sample compared with the control sample.

#### 2.8. Measurement of protein concentration by BCA method

Extraction of total retinal protein: Put retina into EP tube, add 100  $\mu$ L RIPA tissue lysate (Hangzhou Haoxin Biotechnology Co., Ltd., China) and 1  $\mu$ L phenylmethylsulfonyl fluoride (Shanghai Jizhi Biochemical Technology Co., Ltd., China), and make ultrasonic homogenate. Centrifuge (4 °C, 10 000 r/min) for 10 min, absorb the supernatant, transfer it to the new EP tube, and store in reserve at - 80 °C.

Measurement of protein concentration: dissolve BCA powder with 1 mL saline, and set different concentrations of BCA working fluid according to the instructions. 20  $\mu$ L diluted protein samples were added to the labeled 96-well plate. Each sample was equipped with three parallel holes, each hole was mixed with 200  $\mu$ L BCA working fluid, and then put into the incubator (37 °C) for 30 min. The absorbance was measured by fully automatic enzyme labels (Molecular Devices, USA). The standard curve was drawn from the absorbance of the working fluid, and the protein concentration of the sample was calculated.

#### 2.9. Detection of the expression of VEGF in mouse retina by Western blot

Preparation of separating and concentrating gum: 4.7 mL distilled water, 2.6 mL 30% acrylamide, 2.5 mL 1.5 M Tris-HCl, 50  $\mu$ L 10% SDS, 0.1 mL 10% ammonium persulfate and 4  $\mu$ L TEMED were added sequentially in the test tube, and the evenly mixed. Slowly pour into two glass splints cleaned aseptically and wait for separation and gelation. In another test tube, 3.44 mL distilled water, 0.83 mL 30% acrylamide, 0.63 mL 1 M Tris-HCl (pH 6.8), 50  $\mu$ L 10% SDS, 50  $\mu$ L 10% ammonium persulfate and 5  $\mu$ L TEMED were added sequentially and mixed evenly. Slowly pour into the upper layer of the separating glue between the glass panels, and insert the Teflon toothcomb vertically into the glass splint, waiting for the concentrated glue to solidify.

Electrophoresis: Add the protein to the EP tube, centrifuge, boil in boiling water for 5 min, denature the protein, and cool it on ice. Samples of protein (20  $\mu$ g/pore) to be tested were added into the sample pore. Connecting the power supply, the gel concentrate was electrophoretized at a constant voltage of 8 V. When the protein electrophoresis was transferred to the gel separator (a red line appeared), it was changed to a constant voltage of 120 V. When the protein electrophoresis was transferred to 1 cm at the lower edge of the gel separator, the gel electrophoresis could be completed.

Transferring film and sealing: according to the protein sample to be tested, the gel in the film transfer area was selected and immersed in formaldehyde. 2 min later, it was removed and put into distilled water. After 1 min, it was removed and placed in the transfer solution. After 3 min, it was removed. Put the filter paper, gel, PVDF film and filter paper in order, and avoid the bubbles. Turn on the power supply, constant current 200 mA, voltage 15 V for 20 min. Remove the PVDF film, add the sealing liquid (5% BSA) and mix evenly, and place it overnight under 4 °C.

Antibody incubation: Take out PVDF membrane and rinse it in TBST solution three times for 5 min each time. Add an anti-dilution solution and shake it lightly on a shaking bed (4 °C) overnight. Rinse it three times with TBST solution for 5 min each time. Anti-rabbit/rat diluent (1:10000) was added and incubated at room temperature for 2 h. Chemi Doc XRS gel image acquisition system (Bio-Rad, USA) was scanned for preservation. Using  $\beta$ -actin as internal parameter index, the gray value of protein bands was calculated.

#### 2.10. Data analysis

SPSS22.0 software was used for statistical analysis of data. All quantitative data were tested for normal distribution and

**Table 1**  
Evaluation results of fluorescence leakage in choroidal lesions of mice.

Groups	7th day (mm <sup>2</sup> )	14th (mm <sup>2</sup> )	21st (mm <sup>2</sup> )
Group A	0	0	0
Group B	5.534 ± 0.674	3.357 ± 0.527	2.528 ± 0.468
Group C	3.513 ± 0.539	1.502 ± 0.326	1.006 ± 0.214

homogeneity of variance, which were expressed as mean ± standard deviation ( $\bar{x} \pm s$ ). Single factor analysis of variance was used for comparison among groups. Least significant difference (LSD) test was used for normal distribution and homogeneous variance, and SNK-q test was used for variance. Pearson correlation analysis was used to analyze the correlation between the two parameters, and the difference was significant when  $P < 0.05$ .

### 3. Results and discussion

#### 3.1. Evaluation results of fluorescence leakage in choroidal lesions of mice

The fluorescence leakage of choroidal lesions in mice was assessed by fundus fluorescence angiography. The results are shown in Table 1 and Fig. 1. It can be seen that the fluorescence leakage area of mice in group B and group C decreased significantly with the passage of time, and the difference was statistically

significant ( $P < 0.05$ ). On the 7th, 14th and 21st day after modeling, compared with group B, the fluorescence leakage area of group C mice was significantly reduced, and the difference was statistically significant ( $P < 0.05$ ).

#### 3.2. Observation results of morphological changes of retinal vessels and histopathological changes of eyeball in mice

The morphological changes of retinal blood vessels in mice were observed by retinal paving. As shown in Fig. 2, the retinal blood vessels in group A were normal, clear, no ischemia and no perfusion area, no neovascularization clusters and vascular leakage. In group B, the retinal blood vessels showed more layers and branches, and the movement was disordered. There was a large area of ischemia without perfusion, accompanied by abundant neovascularization clusters and capillaries. Compared with group B, the retinal vascular stratification and branches in group C were significantly reduced, the course was clearer, the area of ischemic no-perfusion area was smaller, and a small number of neovascularization clusters and capillaries could be seen.

The pathological changes of eyeball tissue of mice were observed by HE staining. The results showed that the eyeball tissue structure of group A was normal, and that of group B had fusiform injury of inner and outer retina. Compared with group B, fusiform injury of group C was significantly reduced.

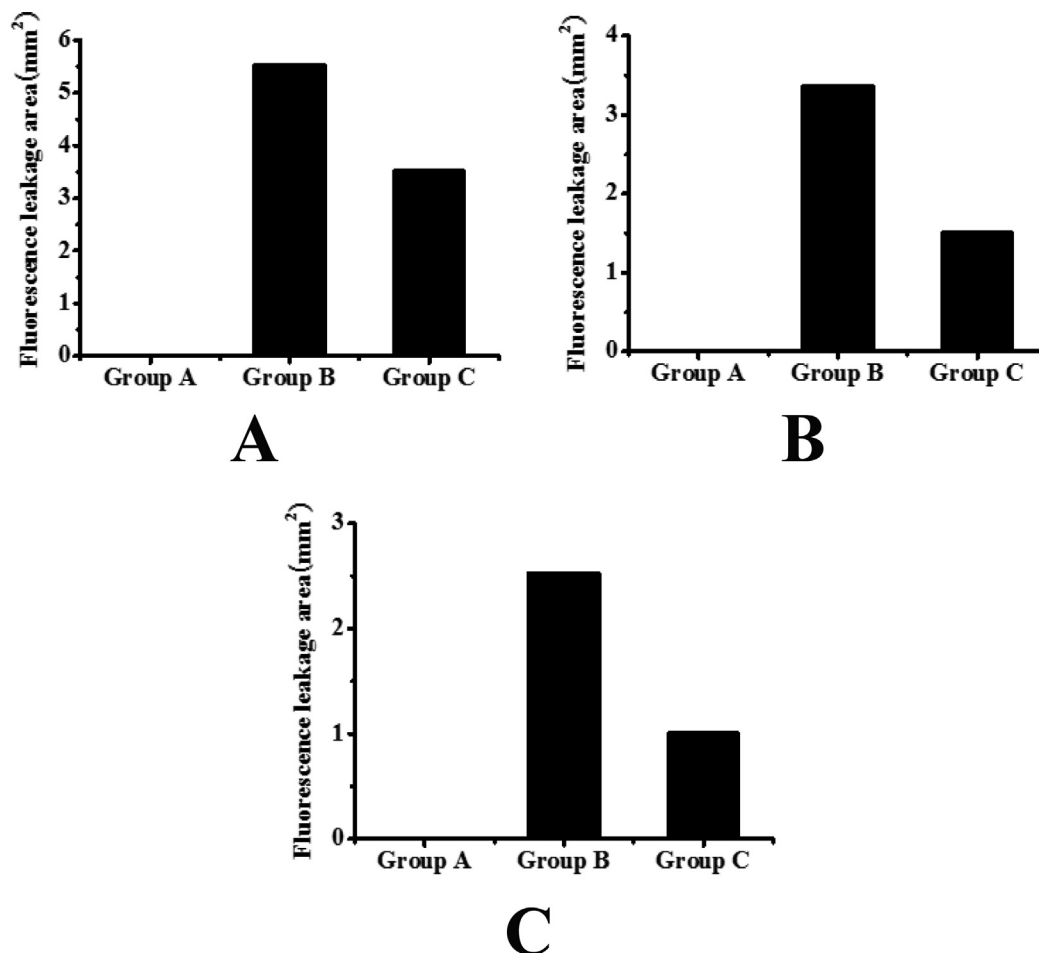


**Fig. 1.** The evaluation results of fluorescence leakage degree in choroidal lesion area of mice (A: the evaluation result of fluorescence leakage degree in choroidal lesion area of mice on the 7th day after model establishment; B: the evaluation result of fluorescence leakage degree in choroidal lesion area of mice on the 14th day after model establishment; C: the evaluation result of fluorescence leakage degree in choroidal lesion area of mice on the 21st day after model establishment).

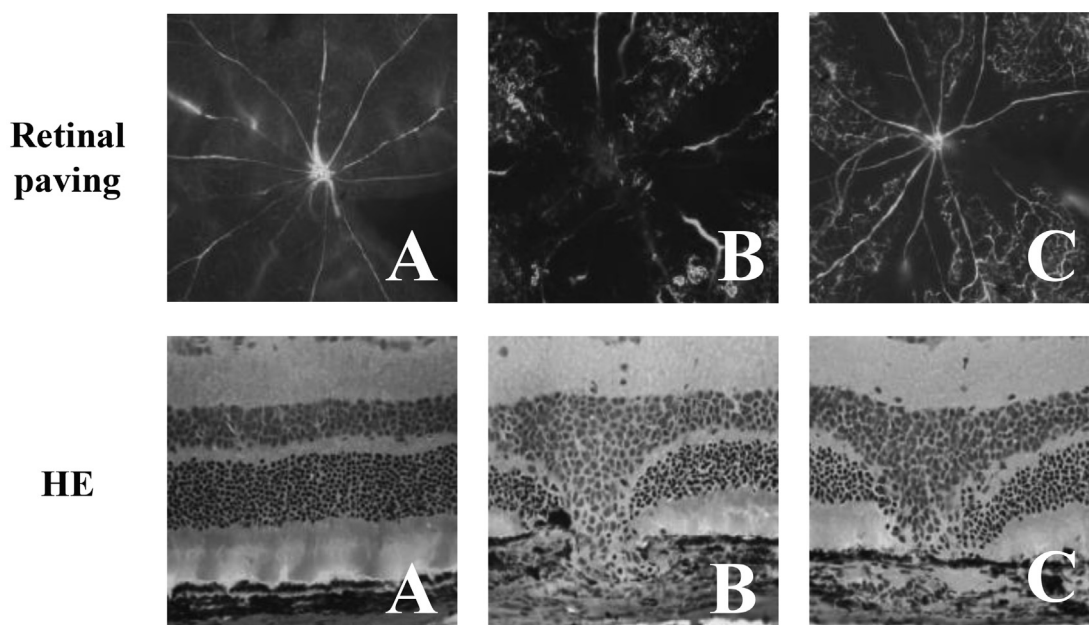


**Fig. 2.** Morphological changes of retinal vessels in mice and histopathological changes of eyeball in mice (Retinal paving was the result of morphological changes of retinal vessels in mice; HE was the result of histopathological changes of eyeball in mice).

**Table 2**  
Detection of mRNA expression of VEGF in mice retina.

Groups	The expression of mRNA of VEGF
Group A	0.05 ± 0.01
Group B	0.75 ± 0.10
Group C	0.27 ± 0.04

### 3.3. Detection of mRNA expression of VEGF in mice retina

The mRNA expression of VEGF in the retina of mice was detected by real-time quantitative fluorescent PCR. The results are shown in Table 2 and Fig. 3A. The mRNA expression of VEGF in retina of group A was  $0.05 \pm 0.01$ , that in retina of group B was  $0.75 \pm 0.10$ , and that in retina of group C was  $0.27 \pm 0.04$ . It can be seen that compared with group A, the mRNA expression of VEGF in retina of group B mice was significantly increased, and the difference was statistically significant ( $P < 0.05$ ). Compared with group B, the mRNA expression of VEGF in retina of mice in group C was significantly decreased, and the difference was statistically significant ( $P < 0.05$ ).

### 3.4. Detection of the protein expression of VEGF in mice retina

The expression of VEGF protein in the retina of mice was detected by Western blotting. The results are shown in Table 3 and Fig. 3B. The expression of retinal VEGF in group A was  $0.49 \pm 0.02$ , that in group B was  $1.27 \pm 0.08$ , and that in group C was  $0.61 \pm 0.06$ . It can be seen that compared with group A, the protein expression of VEGF in retina of group B mice was significantly increased, and the difference was statistically significant ( $P < 0.05$ ). Compared with group B, the protein expression of VEGF in retina of group C mice was significantly decreased, and the difference was statistically significant ( $P < 0.05$ ).

## 4. Discussion

Fundus fluorescein angiography and immunostaining are the keys to identifying whether the CNV model is successfully

modeled. Increasing the traceability of experimental data and the characteristics of continuous observation have laid the foundation for the rapid evaluation of drugs through preclinical studies (Mierra et al., 2019). The therapeutic effect and mechanism of levotinin on CNV in mice were studied. 45 healthy C57BL/6 mice were randomly divided into three groups: control group, model group and levotinin group. A mouse model of CNV was established by fundus fluorescence. Angiography was used to observe the fluorescence leakage of choroidal lesions, retinal paving was used to observe the morphological changes of retinal vessels, and HE staining was used to observe the pathological changes of eyeball. The results showed that on the 7th, 14th and 21st day after modeling, compared with group B, the fluorescence leakage area of group C mice was significantly reduced, and the difference was statistically significant ( $P < 0.05$ ). Compared with group B, the morphology of retinal vessels in group C was significantly improved. Group A mice had normal eyeball structure, group B mice had visible spindle injury in the inner and outer retina, while compared with group B, group C mice had significantly reduced spindle injury. It shows that levotinin has obvious therapeutic effect on CNV, and the experimental results have reached the expected effect. This is also consistent with the therapeutic effect of levotinin on anti-angiogenesis of tumors shown in the study (Tarallo et al., 2020). The above results lay a credible and direct evidence basis for evaluating the effect of levotinin on CNV. The vascular fluorescence staining on the stretched preparation of mouse choroid provides clear evidence that levotinin inhibits CNV angiogenesis from molecular markers, which is intuitive and statistical.

The formation of retinal neovascularization is a complex process involving multiple growth factors. For the treatment of retinal neovascular eye disease, anti-VEGF treatment is more accurate. But until now, anti-VEGF treatment alone has not completely inhibited retinal neovascularization. It indicates that there is a substance that is independent of VEGF as well as its upstream and downstream pathways, which promotes the formation of neovascularization (Qi et al., 2019). Tyrosine kinase has multiple regulatory functions in the process of cell physiology, and participates in processes including metabolism, growth, differentiation, and apoptosis (Woodward et al., 2019). Many investigations have shown

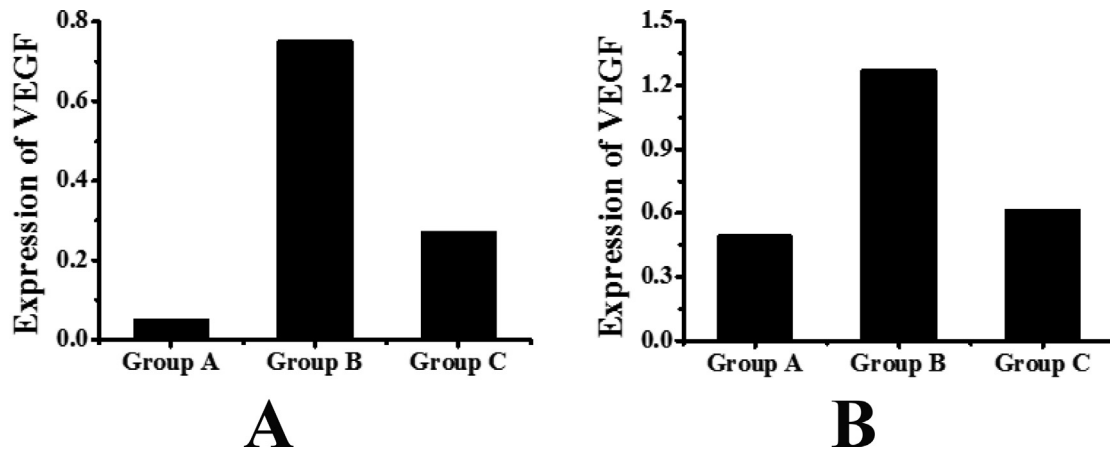


**Fig. 3.** Detection results of the expression of VEGF in mice retina (A: the detection result of the expression of VEGF gene; B is the detection result of the protein expression of VEGF).

**Table 3**

Detection of the protein expression of VEGF in mice retina.

Groups	Protein expression of VEGF
Group A	0.49 ± 0.02
Group B	1.27 ± 0.08
Group C	0.61 ± 0.06

that appropriate receptor-type tyrosine kinase monoclonal antibodies and inhibitors can effectively inhibit tumor cell differentiation, apoptosis, and angiogenesis (Casalino et al., 2019; Karacorlu et al., 2019; Zhu et al., 2019). In this study, the mRNA expression of VEGF in mice retina was detected by Real-time PCR, and the protein expression of VEGF in mice retina was detected by Western blot. The results showed that compared with group A, the mRNA expression of VEGF in retina of group B mice was significantly increased, and the difference was statistically significant ( $P < 0.05$ ), while compared with group B, the mRNA expression of VEGF in retina of group C mice was significantly decreased, and the difference was statistically significant ( $P < 0.05$ ). Compared with group A, the protein expression of VEGF in retina of group B mice was significantly increased, and the difference was statistically significant ( $P < 0.05$ ); compared with group B, the protein expression of VEGF in retina of group C mice was significantly decreased, and the difference was statistically significant ( $P < 0.05$ ). These results suggest that levotinic can inhibit the high expression of VEGF in CNV. The investigation by Li et al. (Li et al., 2020) showed that tyrosine kinase inhibitors may inhibit angiogenesis of endometrial tissue in the peritoneum by inhibiting the expression of VEGF-A and HIF-1 $\alpha$  (Li et al., 2020). It is almost consistent with the results of this study.

In summary, levotinic has a significant therapeutic effect on retinal choroidal neovascularization, and its mechanism may be achieved by inhibiting the high expression of VEGF in retinal choroidal neovascularization.

## 5. Conclusion

In this study, a mouse model of CNV was established to study the therapeutic effect of levotinic and its mechanism. Levotinic has obvious therapeutic effect on CNV, which may be achieved by inhibiting the high expression of VEGF in CNV. However, there are also some shortcomings in the process of this study, such as the small amount of data collected from the samples, which leads

to a certain degree of deviation of the results. Therefore, in the later research process, the data capacity will be further increased to make the results more valuable.

## References

- Aggarwal, K., Agarwal, A., Sharma, A., et al., 2019. Detection of type 1 choroidal neovascular membranes using optical coherence tomography angiography in tubercular posterior uveitis. *Retina* 39 (8), 1595–1606.
- Breazzano, M.P., Yannuzzi, L.A., Spaide, R.F., 2020. Characterizing retinal-choroidal anastomosis in macular telangiectasia type 2 with optical coherence tomography angiography. *Retina* 40 (1), 92–98.
- Casalino, G., Sivagnanavel, V., Dowlut, S., et al., 2019. Spontaneous retinal pigment epithelial tear in type 2 choroidal neovascularization: repair mechanisms following anti-VEGF therapy. *Int. J. Retina Vitreous* 5 (1), 4.
- Choudhary, M., Safe, S., Malek, G., 2018. Suppression of aberrant choroidal neovascularization through activation of the aryl hydrocarbon receptor. *Biochimica et Biophysica Acta (BBA)-Molecular Basis of Disease* 1864 (5), 1583–1595.
- Farinha, C., Santos, T., Santos, A.R., et al., 2020. Optical coherence tomography leakage in neovascular age-related macular degeneration: identification of choroidal neovascularization activity by location and quantification of abnormal fluid under anti-vascular endothelial growth factor therapy. *Retina* 40 (5), 881.
- Gualino, V., Tadayoni, R., Cohen, S.Y., et al., 2019. Optical coherence tomography, fluorescein angiography, and diagnosis of choroidal neovascularization in age-related macular degeneration. *Retina* 39 (9), 1664.
- Haas, A.M., Stattin, M., Ahmed, D., et al., 2020. Development of secondary choroidal neovascularization in focal choroidal excavation of punctate inner choroidopathy. *Ocular Immunol. Inflammation* 28 (1), 20–25.
- Hachana, S., Fontaine, O., Sapieha, P., et al., 2020. The effects of anti-VEGF and kinin B1 receptor blockade on retinal inflammation in laser-induced choroidal neovascularization. *Br. J. Pharmacol.* 177 (9), 1949–1966.
- Karacorlu, M., Muslubas, I.S., Arf, S., et al., 2019. Membrane patterns in eyes with choroidal neovascularization on optical coherence tomography angiography. *Eye* 33 (8), 1280–1289.
- Kiel, C., Berber, P., Karlstetter, M., et al., 2020. A circulating microRNA profile in a laser-induced mouse model of choroidal neovascularization. *Int. J. Mol. Sci.* 21 (8), 2689.
- Kumar, A., Vohra, R., Agrawal, S., et al., 2018. Characterization of idiopathic choroidal neovascularization using fluorescein angiography, indocyanine green angiography, and optical coherence tomography angiography. *Ophthalmic Surgery Lasers Imaging Retina* 49 (7), 516.
- Li, L., Zhu, M., Wu, W., et al., 2020. Brivanib, a multitargeted small-molecule tyrosine kinase inhibitor, suppresses laser-induced CNV in a mouse model of neovascular AMD. *J. Cell. Physiol.* 235 (2), 1259–1273.
- Lima, L.H., Farah, M.E., Gum, G., et al., 2019. Correction to: Sustained and targeted episcleral delivery of celecoxib in a rabbit model of retinal and choroidal neovascularization. *Int. J. Retina Vitreous* 5 (1), 3.
- Mandal, N., Lotery, A.J., 2019. Multimodal imaging of late-onset retinal degeneration complicated by bilateral choroidal neovascularization. *Eye* 33 (6), 1020–1027.
- Miere, A., Butori, P., Cohen, S.Y., et al., 2019. Vascular remodeling of choroidal neovascularization after ANTI-VASCULAR endothelial growth factor therapy visualized on optical coherence tomography angiography. *Retina* 39 (3), 548–557.

- Moult, E.M., Alibhai, A.Y., Rebhun, C., et al., 2020. Spatial distribution of choriocapillaris impairment in eyes with choroidal neovascularization secondary to age-related macular degeneration: a quantitative OCT angiography study. *Retina* 40 (3), 428–445.
- Murakawa, S., Maruko, I., Kawano, T., et al., 2019. Choroidal neovascularization imaging using multiple en face optical coherence tomography angiography image averaging. *Graefes Archive Clin. Experiment. Ophthalmol.* 257 (6), 1119–1125.
- Park, W., Baek, Y.Y., Kim, J., et al., 2019. Arg-Leu-Tyr-Glu suppresses retinal endothelial permeability and choroidal neovascularization by inhibiting the VEGF receptor 2 signaling pathway. *Biomol. Therapeutics* 27 (5), 474.
- Philip, S., Xu, X., Laud, K.G., et al., 2019. Choroidal neovascularization in an adolescent with RDH12-associated retinal degeneration. *Ophthalmic Genet.* 40 (4), 362–364.
- Qi, J.H., Bell, B., Singh, R., et al., 2019. Sorsby fundus dystrophy mutation in tissue inhibitor of metalloproteinase 3 (TIMP3) promotes choroidal neovascularization via a fibroblast growth factor-dependent mechanism. *Sci. Rep.* 9 (1), 1–14.
- Rust, R., Gantner, C., Schwab, M.E., 2019. Pro- and antiangiogenic therapies: current status and clinical implications. *FASEB J.* 33 (1), 34–48.
- Saurabh, K., Roy, R., Thomas, N.R., et al., 2018. Concurrent management of myopic choroidal neovascularization and rhegmatogenous retinal detachment with intravitreal antivascular endothelial growth factor during primary retinal detachment repair. *Indian J. Ophthalmol.* 66 (3), 472–474.
- Savastano, M. C., Rispoli, M., Lumbroso, B., 2019. Choroidal juxtapapillary neovascularization regression in multiple evanescent white dot syndrome by optical coherence tomography angiography: a case report. *J. Medical Case Reports* 13 (1), 274.
- Schwarzer, P., Kokona, D., Ebnetter, A., et al., 2020. Effect of inhibition of colony-stimulating factor 1 receptor on choroidal neovascularization in mice. *Am. J. Pathology* 190 (2), 412–425.
- Simhaee, D., Dolz-Marco, R., Freund, K.B., 2020. Choroidal nevi with focal choroidal excavation and polypoidal choroidal neovascularization. *Retinal Cases Brief Rep.* 14 (1), 39–43.
- Tarallo, V., Iaccarino, E., Cicatiello, V., et al., 2020. Oral delivery of a tetrameric tripeptide inhibitor of VEGFR1 suppresses pathological choroid neovascularization. *Int. J. Mol. Sci.* 21 (2), 410.
- Wang, Y., Liu, C.H., Ji, T., et al., 2019. Intravenous treatment of choroidal neovascularization by photo-targeted nanoparticles. *Nat. Commun.* 10 (1), 1–9.
- Woodward, D.F., Wang, J.W., Ni, M., et al., 2019. In vivo choroidal neovascularization and macrophage studies provide further evidence for a broad role of prostacyclin in angiogenesis. *J. Ocul. Pharmacol. Ther.* 35 (2), 98–105.
- Xiao, M., Dai, C., Li, L., et al., 2020. Evaluation of retinal pigment epithelium and choroidal neovascularization in rats using laser-scanning optical-resolution photoacoustic microscopy. *Ophthalmic Res.* 63 (3), 271–283.
- Zhao, M., Mantel, I., Gelize, E., et al., 2019. Mineralocorticoid receptor antagonism limits experimental choroidal neovascularization and structural changes associated with neovascular age-related macular degeneration. *Nat. Commun.* 10 (1), 1–13.
- Zhu, M., Jiang, L., Yuan, Y., et al., 2019. Intravitreal Ets1 siRNA alleviates choroidal neovascularization in a mouse model of age-related macular degeneration. *Cell Tissue Res.* 376 (3), 341–351.